The Abdus Salam
International Centre for Theoretical Physics

United Nations
Educational, Scientific and
Cultural Organization

IAEA
International Atomic Energy Agency

1953-49

International Workshop on the Frontiers of Modern Plasma Physics

14 - 25 July 2008

Finite Larmor Radius Effects on 3-D Blobs in the SOL.

D. Jovanovic
Institute of Physics, Belgrade, Republic of Serbia

Finite Larmor Radius Effects on 3-D Blobs in the SOL

Dušan Jovanović

Institute of Physics, Belgrade, Serbia

International Workshop on the Frontiers of Modern Plasma Physics, 14 - 25 July 2008, Abdus Salam ICTP, Trieste

Collaboration

Padma K. Shukla
Ruhr University, Bocum, Germany

Francesco Pegoraro
Physics Department, Universita di Pisa, Italia

Special thanks to

Umberto de Angelis
University Federico II, Naples, Italy

Introduction

- The particle and the energy transports in the scrape-off layer (SOL) of tokamak are intermittent, due to the presence of coherent filamentary plasma structures.
- These structures, called **blobs**, are elongated along the magnetic field and much smaller (cm-sized) in the perpendicular direction.
- Blobs propagate radialy with a velocity in the thermal range (~1000 m/s).
- Plasma inside the blobs is an order of magnitude denser, and much hotter than the surrounding plasma.
- Blobs result from the leaking of the dense and hot core plasma across the last closed magnetic surface into the SOL, due to the magnetic curvature driven instabilities (Raleigh-Taylor, interchange, ballooning) in the core region.
- Turbulence at the core edge is strongly affected e. g. by the dissipations.
- Low dissipation $\Rightarrow$ the condensation of energy arising from the nonlinear interactions preferentially gives rise to zonal structures $\Rightarrow$ transport barrier $\Rightarrow$ good for confinement.
- Stronger dissipation $\Rightarrow$ streamer structures $\Rightarrow$ detachment from the core $\Rightarrow$ breakup into blobs.
- Dynamics of individual blobs affects the SOL plasma transport, confinement, erosion, and even the structural stability of the first wall.
- Blob dynamics strongly affected by dissipative effects $\Rightarrow$ they move radialy outwards, carried by magnetic curvature down the density gradient.

Highlights

- A new three-dimensional model for the warm-ion turbulence at the tokamak edge plasma and in the scrape-off layer is proposed, and used to study the dynamics of plasma blobs in the scrape-off layer.
- The model is based on the nonlinear interchange mode, coupled with the nonlinear resistive drift mode, in the presence of the magnetic curvature drive, the density inhomogeneity, the electron dynamics along the open magnetic field lines, and the electron-ion and electron-neutral collisions.
- Within the present model, the effect of the sheath resistivity decreases with the distance from the wall, resulting in the bending and the break up of the plasma blob structure.
- Numerical solutions exhibit the coupling of interchange modes with nonlinear drift modes, causing the collapse of the blob in the lateral direction, followed by a clockwise rotation and radial propagation.
- The symmetry breaking, caused both by the parallel resistivity and the finite ion temperature, introduces a poloidal component in the plasma blob propagation, while the overall stability properties and the speed are not affected qualitatively.

Introduction (contd.)

- Leaking of dense and hot core plasma into SOL region (cold and tenuous) due to ballooning/interchange turbulence.
- Intermittent convection in the boundary of DIII-D:

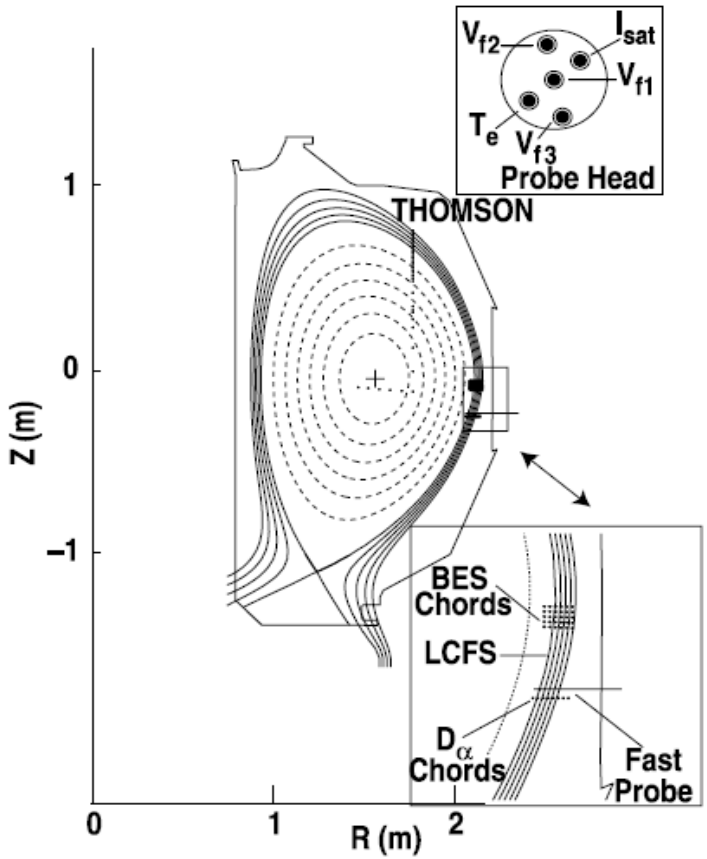

Fig. 2. Poloidal cut of DIII-D showing the magnetic geometry and some relevant diagnostics. Two insets show (top) the scanning probe tip geometry and (bottom) the BES diagnostic geometry.

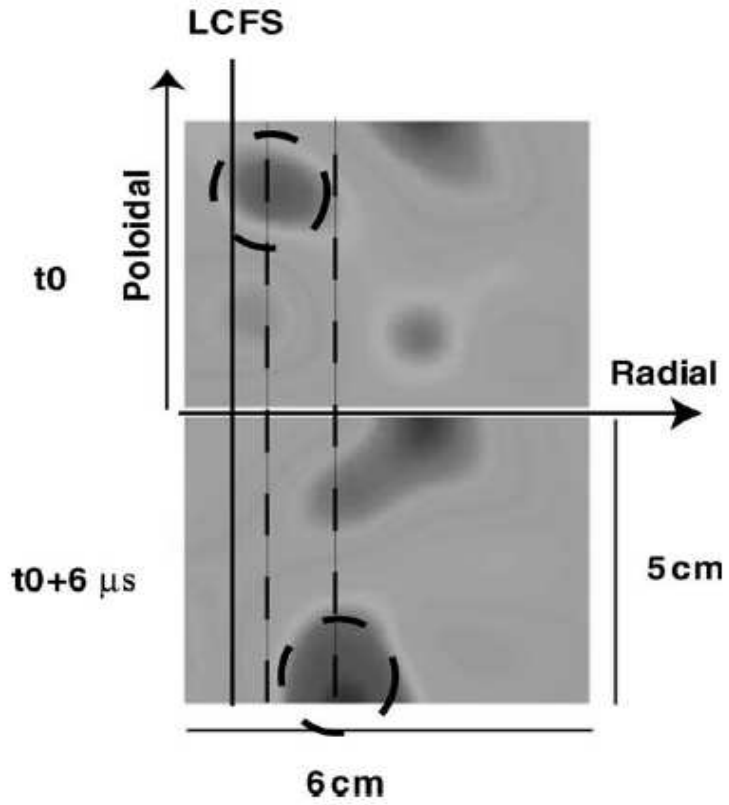

Fig. 4. Two frames from BES showing 2-D density plots. There is a time difference of 6 μs between frames. A particular structure is marked with a dashed circle, and shown in both frames, clearly highlighting poloidal and radial motion.

J.A. Boedo et al. / Journal of Nuclear Materials 313–316 (2003) 813–819

Structures in the scrape-off layer of Alcator C-Mod

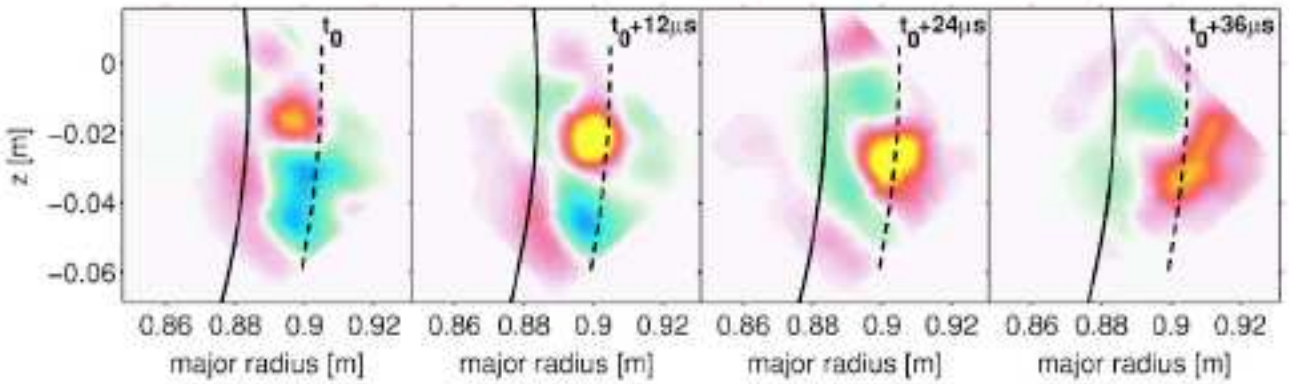

FIG. 9. (Color online) For consecutive ultrafast camera frames of the D_α emission intensity fluctuations in a poloidal cross section. Red and yellow colors correspond to positive fluctuation amplitudes, green and blue to negative. The separatrix position is indicated as the black solid line, the projection of the limiter edge as the dashed line. Shown is the evolution of a long living blob from its formation close to the separatrix to its decay in the limiter shadow.

Gas puff imaging of blobs in Alcator C-Mod boundary

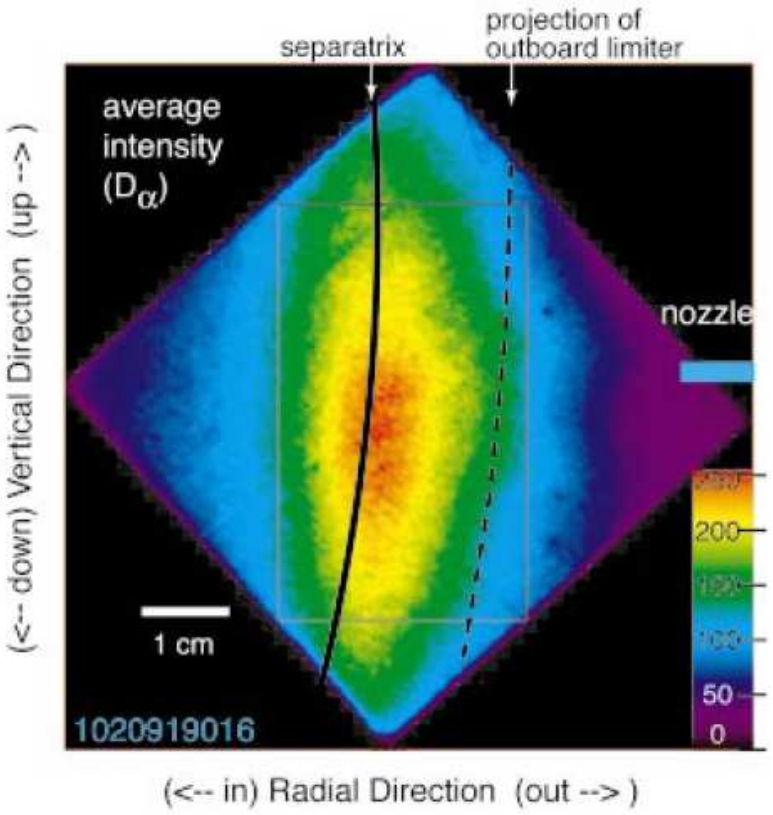

FIG. 1. (Color) The time-averaged image of D_α brightness from the gas puff on the outboard midplane. The X-section is the plane perpendicular to the local field. Also shown are the separatrix, the projection of the outboard limiter, and the rectangular box inside of which the k_{pol} spectra and L_{pol} are calculated. The poloidal variation in the average image is due to the poloidal distribution of the gas puffed from the nozzle, whose location is also shown.

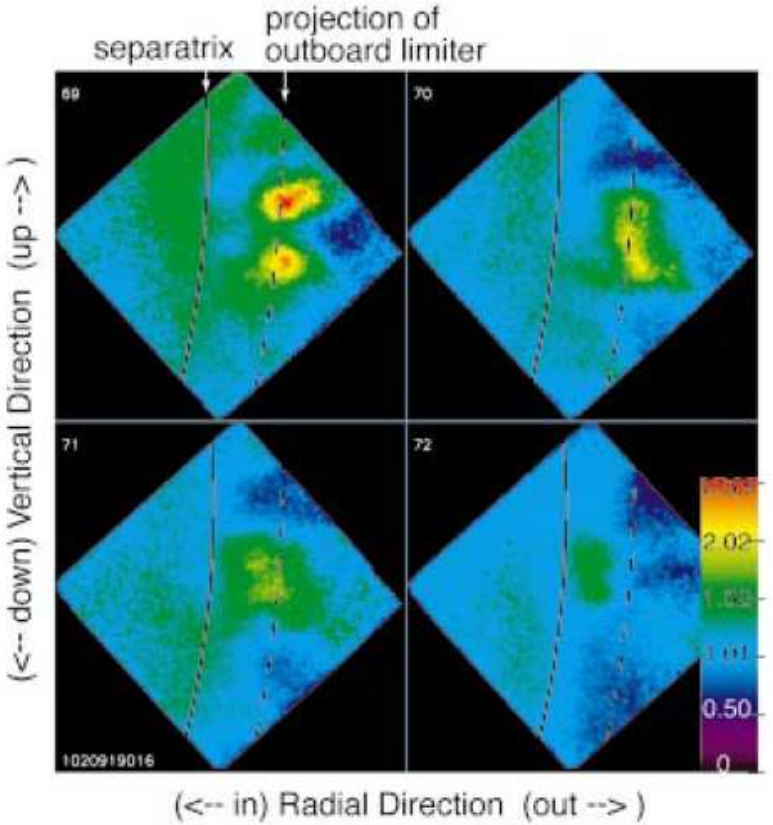

FIG. 2. (Color) Four consecutive "normalized" images calculated by dividing each 2 μs snapshot by the time-averaged image. Two large-amplitude fluctuations—blobs—are seen in the first image. Each of the other three images shows smaller amplitude structures existing primarily outside the separatrix, as well as emission "holes," where the snapshot emission is less than the average. The scale shows the emission relative to the average.

Interchange turbulence in the TCV scrape-off layer

- Probe measurements of electrostatic plasma fluctuations in the scrape-off layer (SOL) of the TCV tokamak are compared with the results from two dimensional interchange turbulence simulations.
- Agreement is found for the radial variation of statistical moments and temporal correlations.
- Turbulent transport in the SOL is due to radial advection of blob-like filamentary structures.

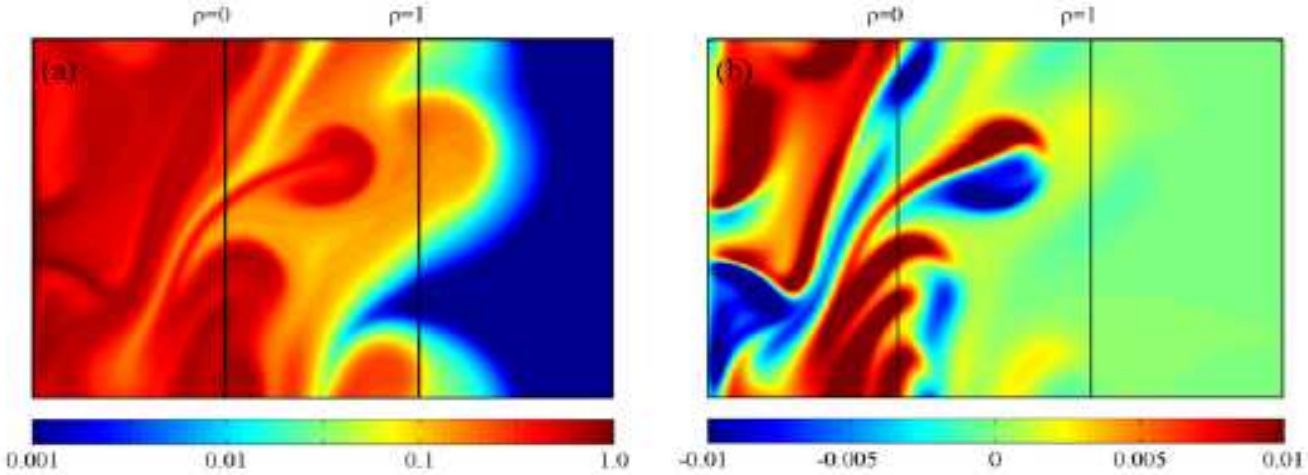

Figure 2. Spatial structure of (*a*) the particle density and (*b*) the electric drift vorticity in the interchange turbulence simulation. Exponential contour levelling is used for the particle density in order to reveal its spatial structure in all regions.

O E Garcia Plasma Phys. Control. Fusion **48** (2006) L1–L10

Introduction (contd.)

Bisai et al.
Phys. Plasmas, Vol. 11, No. 8, August 2004

- FIG 8. Detachment of density structure and its radial and poloidal motions.
- The detached structure forms like a blob and moves in the radial and as well as poloidal direction. The movement is shown by horizontal and vertical lines. The time difference between upper and lower figures is about 200 normalized time.

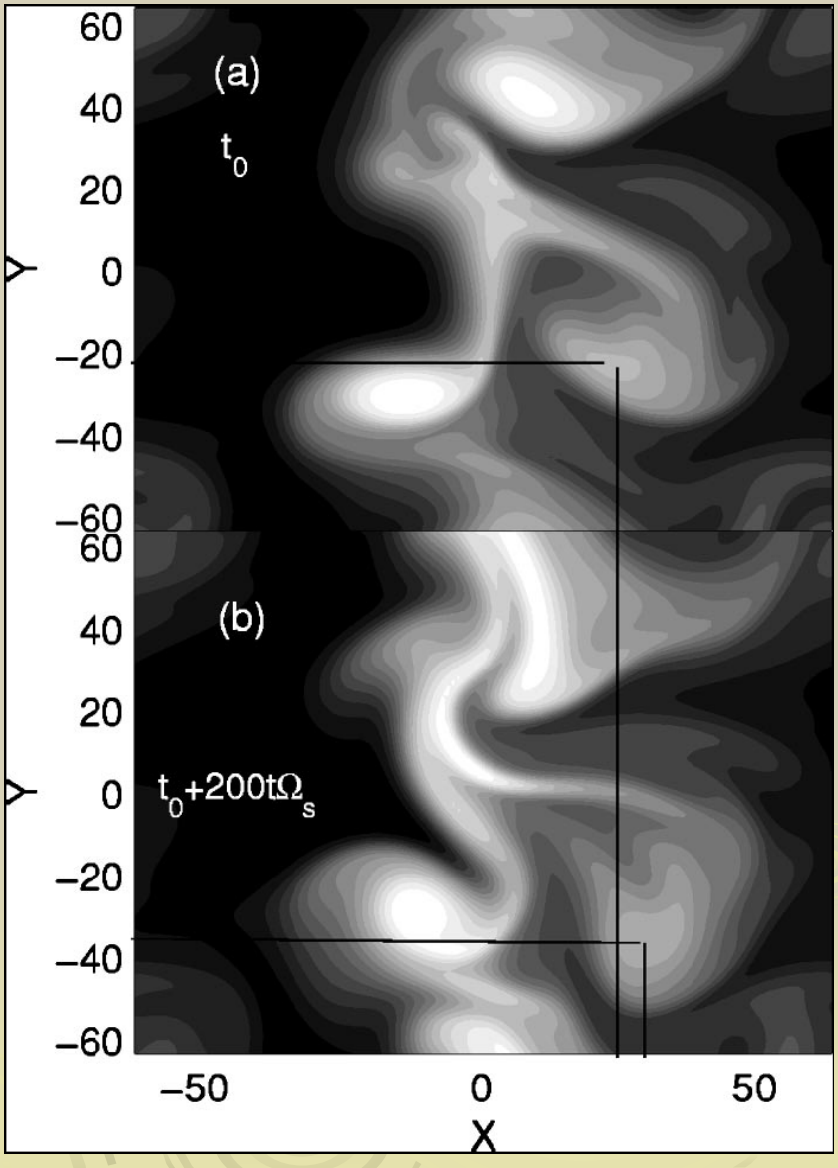

FLR effects, 3-D effects

- $T_e \approx T_i$ in the SOL, but most theories/simulations consider cold ions. We include full Braginskii stress-tensor response.
- Parallel transport is crucial for ballooning modes. It also introduces the coupling with resistive drift mode. Usually oversimplified in earlier blob theories. 3-D effects often included via an effective wavenumber, corresponding to an essentially linear response.
- We use a rigorous separation of rapid and slow parallel variables in a fully NL regime. For simplicity, we neglect the temperature inhomogeneity $\Rightarrow$ no coupling to ITG mode.
- We study only the propagation of blobs in SOL, but our model equations with the appropriate boundary conditions allow also the study of the blob generation at the core edge.
- NL 3-D effects $\Rightarrow$ increase of the blob velocity with the distance from the wall $\Rightarrow$ bending and break up of the structure.
- 3-D effects break the symmetry of the purely interchange structures (monopolar density, dipolar electrostatic potential). Rotation and collapse in the perpendicular direction observed. Tripolar structure of the electrostatic potential.

Hydrodynamic description

$$\frac{\partial n_\alpha}{\partial t} + \nabla \cdot \left(n_\alpha \vec{v}_\alpha \right) = \gamma_{e,n}^{(ion)} \, n_e n_n ,$$

$$\left(\frac{\partial}{\partial t} + \vec{v}_\alpha \cdot \nabla \right) \vec{v}_\alpha = \frac{q_\alpha}{m_\alpha} \left(-\nabla \phi + \vec{v}_\alpha \times \vec{B} \right) - \frac{1}{m_\alpha n_\alpha} \left(\nabla p_\alpha + \vec{e}_l \frac{\partial \pi_{\alpha_{l,m}}}{\partial x_m} \right) \mp$$

$$\mp \frac{m_e}{m_\alpha} \gamma_{e,i} \, n_e \left(\vec{v}_e - \vec{v}_i \right) + \eta_\alpha \nabla^2 \vec{v}_\alpha - \gamma_{\alpha,n}^{(sc)} \, n_n \left(\vec{v}_\alpha - \vec{v}_n \right),$$

- $\pi_{l,m}$ is the Braginskii's collisionless stress tensor.
- Particle source $\gamma_{e,n}^{(ion)} n_e n_n$ from the electron impact ionization of the neutrals.
- For Coulomb collisions: $\gamma_{e,i} = \dfrac{\Lambda e^4}{6\sqrt{2}\,\pi^{\frac{3}{2}}\,\varepsilon_0^2\, m_e^{\frac{1}{2}}\, T_e^{\frac{3}{2}}},$
- Small parameters: $\dfrac{m_e}{m_i}, \dfrac{1}{R\nabla_\perp}, \dfrac{\nabla_\parallel}{\nabla_\perp}, \dfrac{\gamma_{e,i}\, n_e}{\Omega_e}, \dfrac{\gamma_{\alpha,n}\, n_n}{\Omega_e}, \dfrac{\eta_\alpha \nabla_\perp^2}{\Omega_i},$

- Drift regime. Perpendicular electron and ion velocities are given by:

$$\vec{v}_{\alpha_\perp} = \vec{v}_{\alpha_{0\perp}} + \delta\vec{v}_{\alpha_P} + \delta\vec{v}_{\alpha_{FLR}} + \delta\vec{v}_{\alpha_C}$$

$$\vec{v}_{\alpha_{0\perp}} = \vec{v}_{E\times B} + \vec{v}_{\alpha_D} \qquad \vec{v}_{E\times B} = \frac{\vec{B}\times\nabla\phi}{B^2}, \qquad \vec{v}_{\alpha_D} = \frac{\vec{B}\times\nabla p_\alpha}{B^2 q_\alpha n_\alpha},$$

$$\delta\vec{v}_{\alpha_P} = \frac{\vec{e}_z}{\Omega_\alpha}\times\left(\frac{\partial}{\partial t} + \vec{v}_{\alpha_{0\perp}}\cdot\nabla\right)\vec{v}_{\alpha_{0\perp}},$$

$$\delta\vec{v}_{\alpha_{FLR}} = -\frac{1}{2q_\alpha n_\alpha B_0}\left\{\left(\nabla_\perp\frac{p_\alpha}{\Omega_\alpha}\cdot\nabla_\perp + \frac{p_\alpha}{\Omega_\alpha}\nabla_\perp^2\right)\vec{v}_{\alpha_{0\perp}} + \left[\left(\vec{e}_z\times\frac{p_\alpha}{\Omega_\alpha}\right)\cdot\nabla\right]\vec{e}_z\times\vec{v}_{\alpha_{0\perp}}\right\},$$

$$\delta\vec{v}_{\alpha_C} = \frac{\vec{e}_z}{\Omega_\alpha}\times\left[\pm\frac{m_e}{m_\alpha}\,\gamma_{e,i}\,n_e\left(\vec{v}_{e_{0\perp}} - \vec{v}_{i_{0\perp}}\right) - \eta_\alpha\nabla_\perp^2\vec{v}_{\alpha_{0\perp}} + \gamma_{\alpha,n}^{(sc)}\,n_n\left(\vec{v}_{\alpha_{0\perp}} - \vec{v}_n\right)\right],$$

Model equations

- Electron continuity (neglect polarization and FLR effects)

$$\left[\frac{\partial}{\partial t}+\frac{1}{B_0}(\vec{e}_z\times\nabla)\cdot\nabla\right]n+\frac{\gamma_{e,i}\,n^2}{\Omega_e B_0}\frac{T_e+T_i}{e}\,\nabla_\perp^2\ln n-\frac{\gamma_{e,n}^{(sc)}\,nn_n}{\Omega_e B_0}\,\nabla_\perp^2\left(\phi-\frac{T_e}{e}\ln n\right)$$

$$+\nabla_\parallel\left(nv_{e\parallel}\right)=\gamma_{e,n}^{(ion)}\,nn_n,$$

- Ion vorticity equation. Use the Boussinesq approximation (neglect $\nabla_\perp n_\alpha$ compared to $n_\alpha\nabla_\perp$).

$$-\frac{T_e+T_i}{eB_0}\left(\frac{1}{L_s}\frac{\partial}{\partial z}-\frac{2}{R}\frac{\partial}{\partial y}\right)n_i+\nabla_\parallel\left(v_{i\parallel}n_i-v_{e\parallel}n_e\right)$$

$$+\frac{n_i}{\Omega_i B_0}\nabla_\perp\left\{\left[\frac{\partial}{\partial t}+\frac{1}{B_0}(\vec{e}_z\times\nabla\phi)\nabla-\eta_i\nabla_\perp^2+\gamma_{i,n}^{(sc)}\,n_n\right]\nabla_\perp\left(\phi+\frac{T_i}{e}\ln n_e\right)\right\}=0.$$

Parallel dynamics 1. Electrons

$$\left[\frac{\partial}{\partial t}+\frac{1}{B_0}\left(\vec{e}_z\times\nabla\phi\right)\cdot\nabla\right]v_{e\parallel}=\frac{e}{m_e}\nabla_\parallel\left(\phi-\frac{T_e}{e}\ln n\right)+\left(\gamma_{e,i}\,n+\gamma_{e,n}^{(sc)}\,n_n\right)v_{e\parallel}.$$

We seek an elongated, quasi 2-D solution, tilted by the angle θ to the toroidal axis, whose projection in the cross-section makes the angle ϑ with the radius

$$\nabla_\parallel=\frac{\partial}{\partial z'}+\tan\theta\;\vec{p}_\perp(x)\cdot\nabla_\perp,\qquad\qquad \vec{p}_\perp(x)=\vec{e}_x\cos\vartheta+\vec{e}_y(x/L_s+\sin\vartheta)$$

Neglect the electron inertia. Separate the z-averaged and rapidly varying parts. Multiply by $\nabla_\parallel$ and integrate along the axis from the wall ($z=0$) to $z=L_\parallel$, where the average parallel velocity is equal to zero,

$$v_{e\parallel}(z=0)=\frac{1}{\gamma_{e,i}\,n+\gamma_{e,n}^{(sc)}\,n_n}\left[\left(\frac{\partial}{\partial z'}+2\tan^2\theta\;\vec{p}_\perp\cdot\nabla_\perp\right)\frac{e}{m_e}\left(\phi-\frac{T_e}{e}\ln n\right)-\gamma_{e,i}\,n\,v_{i\parallel}\right]_{z=L_\parallel}^{0},$$

From the kinetic considerations, at the plasma-wall boundary we have

$$v_{e\parallel}(z=0)=n\,c_s\exp\left\{\frac{e}{T_e}\left[\phi_0-\phi(z=0)\right]\right\},\qquad\qquad \phi_0=\phi^{wall}+\frac{T_e}{e}\ln\left(\frac{T_e}{T_e+T_i}\frac{m_i}{m_e\sqrt{2\pi}}\right).$$

Parallel dynamics 2. Ions

- The ion velocity at the plasma-sheath boundary is found by the integration of an 1-D ion momentum equation

$$v_{i\parallel} = c_s$$

- If the polarization, FLR and collissional effects are of the same order

$$\frac{c_s}{L_\parallel} \sim \frac{\left(m_e/m_i\right)c_s^2}{\gamma_{e,i}\, n + \gamma_{e,n}^{(sc)}\, n_n}\left|\frac{\partial^2}{\partial z^2}\right| \sim \frac{c_s^2}{\Omega_i^2}\left|\frac{d}{dt}\nabla_\perp^2\right|,$$

- the divergence of parallel flows becomes

$$\nabla_\parallel v_{e\parallel} = \frac{c_s}{L_\parallel}\exp\left[-\frac{e\tilde{\phi}\left(z=0\right)}{T_e}\right] + \frac{\left(e/m_e\right)\tan^2\theta}{\gamma_{e,i}\, n + \gamma_{e,n}^{(sc)}\, n_n}\left(\vec{p}_\perp\cdot\nabla_\perp\right)\vec{p}_\perp\cdot\nabla_\perp\left(\phi - \frac{T_e}{e}\ln n\right),$$

$$\nabla_\parallel v_{i\parallel} = c_s/L_\parallel ;$$

Dimensional equations

$$\left[\frac{\partial}{\partial t}+\rho_s^2\Omega_i\left(\vec{e}_z\times\nabla\frac{e\phi}{T_e}\right)\cdot\nabla\right]\ln n=\nu_{src}-\nu_{sink}+\left(D_{e,i}+D_{e,n}\right)\nabla_\perp^2\ln n-D_{e,n}\nabla_\perp^2\frac{e\phi}{T_e}$$

$$\nu_{RT}\,\rho_s\left(\frac{\partial}{\partial y}-\frac{R}{2L_s}\tan\theta\,\vec{p}_\perp\cdot\nabla_\perp\right)\ln n-\nu_{sink}\frac{e\phi(z=0)}{T_e}+\nu_\parallel\rho_s^2\left(\vec{p}_\perp\cdot\nabla_\perp\right)^2\left(\frac{e\phi}{T_e}-\ln n\right)$$

$$+\rho_s^2\left[\frac{\partial}{\partial t}+\rho_s^2\Omega_i\left(\vec{e}_z\times\nabla\frac{e\phi}{T_e}\right)\cdot\nabla-\eta_i\nabla_\perp^2+\nu_{i,n}\right]\nabla_\perp^2\left(\frac{e\phi}{T_e}+\tau_i\ln n\right)$$

$$+\tau_i\rho_s^4\Omega_i\left(\vec{e}_z\times\nabla\frac{\partial}{\partial x_i}\frac{e\phi}{T_e}\right)\cdot\nabla\frac{\partial\ln n}{\partial x_i}=0,$$

- Notations:

$$\rho_s = \frac{1}{\Omega_i}\left(\frac{T_e}{m_i}\right)^{\frac{1}{2}}, \quad \tau_i = \frac{T_i}{T_e}, \qquad D_{e,n} = \frac{m_e}{m_i}\,\rho_s^2\,\gamma_{e,n}^{(sc)}\,n_n, \quad D_{e,i} = \frac{m_e}{m_i}\left(1+\tau_i\right)\rho_s^2\,\gamma_{e,i}\,n,$$

$$\nu_{src} = \gamma_{e,n}^{(ion)}\,n_n, \quad \nu_{sink} = \frac{c_s}{L_\parallel}, \quad \nu_{i,n} = \gamma_{i,n}^{(sc)}\,n_n,$$

$$\nu_{RT} = 2\Omega_i\left(1+\tau_i\right)\frac{\rho_s}{R}, \quad \nu_\parallel = \frac{\left|\Omega_e\right|\Omega_i\tan^2\theta}{\gamma_{e,i}\,n+\gamma_{e,n}^{(sc)}\,n_n}.$$

- Consistently with the Bousinesq approximation, we neglected the gradients of $D_{e,i}, D_{e,n}, \vec{p}_\perp, \eta_i$ and $\nu_{e,i}$
- The ion vorticity eq. derived for small ion Larmor radius corrections $\tau_i\,\rho_s^2\,\nabla_\perp^2 \ll 1$

- When the electron and ion temperatures are of the same order, our ion vorticity equation is applicable only for the perturbations whose perpendicular scale is much longer than the ion acoustic length $\rho_s^2\nabla_\perp^2 \ll 1$
- For smaller scales, one may use e. g. the Padé approximation.

Scaling laws & Dimensionless equations

- Our equations are valid if $\varphi \sim \tau_i \rho_s^2 / L_\perp^2 \ll 1$. For blobs we have $n \sim 1$
- For simplicity, neglect the effects of magnetic shear $L_s \gg \max(l, R\tan\theta)$

$$\left[\frac{\partial}{\partial t} + (\vec{e}_z \times \nabla\phi)\cdot\nabla\right] n - D\nabla_\perp^2 n = -\sigma n,$$

$$\left[\frac{\partial}{\partial t} + (\vec{e}_z \times \nabla\phi)\cdot\nabla\right] \nabla_\perp^2 (\phi + \tau n) - \frac{\partial n}{\partial y} + \tau\left(\vec{e}_z \times \nabla \frac{\partial\phi}{\partial x_i}\right)\cdot\nabla \frac{\partial n}{\partial x_i} =$$

$$\chi_0 \phi(z=0) + \chi_2 (\vec{p}_\perp \cdot \nabla_\perp)^2 n + \left(\chi_{2_\perp} \nabla_\perp^2 - \chi_4 \nabla_\perp^4\right)(\phi + \tau n).$$

- The expressions for $\sigma, D, \chi_0, \chi_2, \chi_4$ and τ depend on our choice of the normalizations, i.e. on the appropriate scaling laws.
- One can distinguish four different orderings with respect to the intensities of various dissipation mechanisms, to the blob's temporal and spatial scales, and to the amplitude of electrostatic potential.

Scaling 1. 3-D effects in collisional regime

- Collisional regime is, governed by parallel diffusion, is realized when:

$$\min\left[1,\left(\frac{\nu_{RT}^4}{\nu_{sink}^3\,\Omega_i}\right)^{\frac{1}{5}}\right] \gg \varphi \gg \max\left(\frac{D_{e,i}+D_{e,n}}{\rho_s^2\,\Omega_i},\frac{\eta_i}{\rho_s^2\,\Omega_i}\right).$$

- Then we have:

$$\chi_{2\parallel}=1,\quad \chi_{2_\perp}=(\nu_{i,n}/\nu_{RT})(\nu_\parallel/\Omega_i)^{\frac{1}{2}},\quad \chi_0=\chi_4=0,$$

$$\sigma=(\nu_\parallel/\Omega_i)^{\frac{1}{2}}(\nu_{sink}-\nu_{src})/\nu_{RT},\quad \tau=\tau_i\,\nu_{RT}\,\Omega_i^{\frac{1}{2}}/\nu_\parallel^{\frac{3}{2}},$$

$$D=\nu_{RT}\,(D_{e,i}+D_{e,n})/(\rho_s^2\nu_\parallel^{\frac{3}{2}}\Omega_i^{\frac{1}{2}}).$$

3-D effects in collisional regime

Ion density

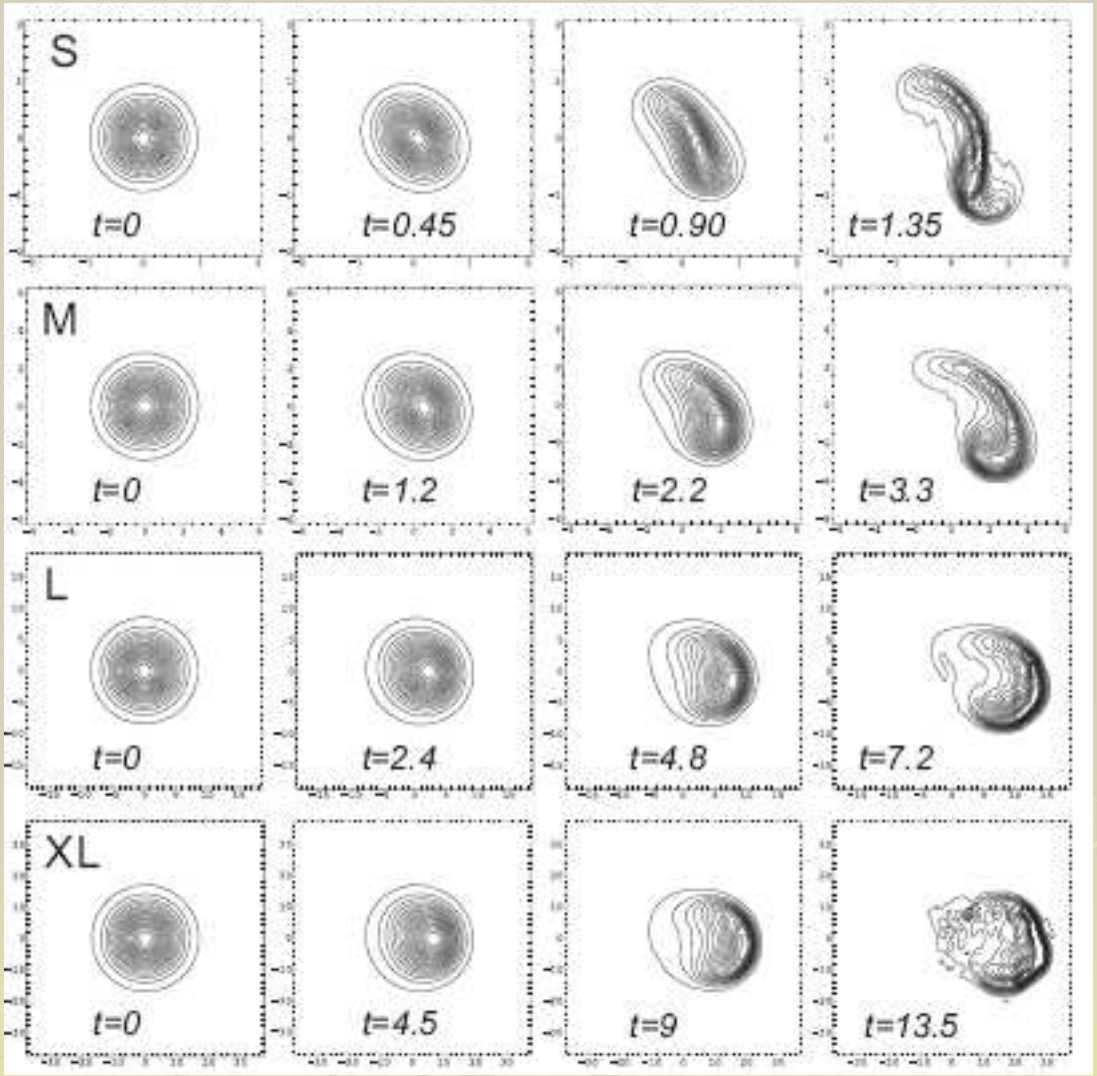

FIG. 1: The effect of the parallel electron dynamics on the blob in the limit of cold ions. The contour plot of the plasma density is displayed, in the **collisional** regime, with the finite pitch of the structure to the magnetic field and finite parallel resistivity, and with negligible collisional effects in the perpendicular direction. From top to bottom are the S (Small, $L_\perp = 0.5$), M (Medium, $L_\perp = 1.5$), L (Large, $L_\perp = 4.5$), and XL (eXtra Large, $L_\perp = 8.5$) blob. The parameters are adopted as $\chi_{2_\parallel} = 1$, $\vartheta = 0$, $D = 10^{-3}$, $\chi_0 = 2 \times 10^{-3}$, $\chi_{2_\perp} = \chi_4 = \gamma = \sigma = \tau = 0$, and the normalizations are defined in Eqs. (38) and (39).

Scaling 2. Inertial regime (no dissipations)

- Inertial (Hamiltonian) regime is realized when:

$$\min\left[1,\left(\frac{\nu_{RT}^4}{\nu_{sink}^3\,\Omega_i}\right)^{\frac{1}{5}},\frac{\nu_{RT}^2\,\Omega_i}{\nu_{i,n}^3},\frac{\nu_{RT}^2\,\Omega_i}{\left(\nu_{sink}-\nu_{src}\right)^3}\right]\gg\varphi\gg\max\left(\frac{\nu_{\blacklozenge}^{\frac{3}{2}}}{\nu_{RT}\,\Omega_i^{\frac{1}{2}}},\frac{D_{e,i}+D_{e,n}}{\rho_s^2\,\Omega_i},\frac{\eta_i}{\rho_s^2\,\Omega_i}\right).$$

- Then we have: $l=\rho_s\left(\frac{\varphi^2\,\Omega_i}{\nu_{RT}}\right)^{\frac{1}{3}}$, $\omega=\left(\frac{\nu_{RT}^2\,\Omega_i}{\varphi}\right)^{\frac{1}{3}}$, arbitrary φ

$$\left[\frac{\partial}{\partial t}+\left(\vec{e}_z\times\nabla\phi\right)\cdot\nabla\right]n=0,$$

$$\left[\frac{\partial}{\partial t}+\left(\vec{e}_z\times\nabla\phi\right)\cdot\nabla\right]\nabla_\perp^2\left(\phi+\tau n\right)-\frac{\partial n}{\partial y}+\tau\left(\vec{e}_z\times\nabla\frac{\partial\phi}{\partial x_i}\right)\cdot\nabla\frac{\partial n}{\partial x_i}=0.$$

Inertial (Hamiltonian) regime

Ion density

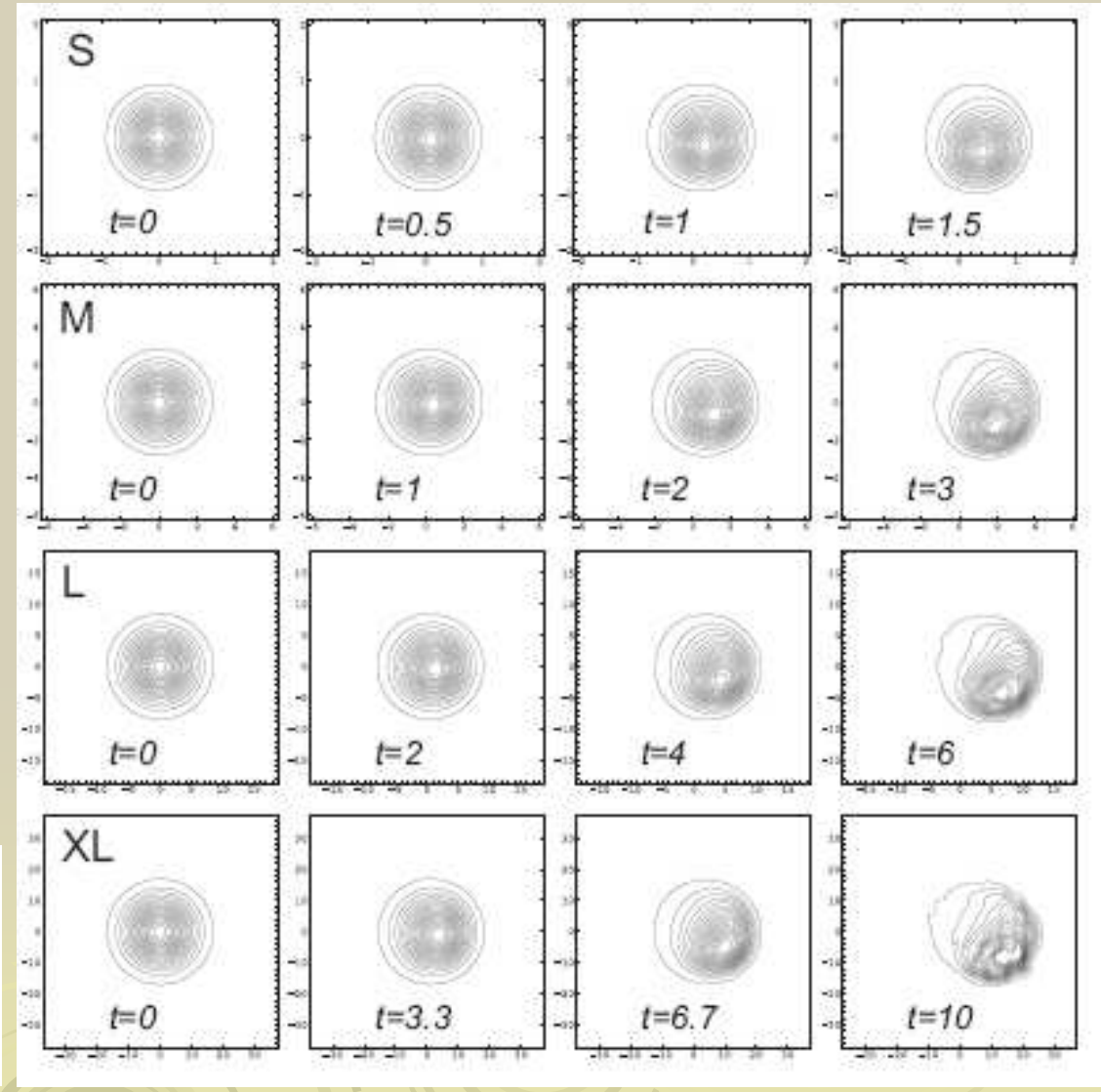

FIG. 2: The effect of the finite ion temperature on the blob density in the **inertial** (or collisionless) regime. The calculations were performed with the following choice of parameters are adopted as $D = 10^{-3}$, $\chi_0 = 2 \times 10^{-3}$, $\chi_{2\perp} = \chi_{2\parallel} = \chi_4 = \gamma = \sigma = 0$, and the dimensionless ion temperature was adopted as $\tau = 1, 3, 12$ and 25 for the S, M, L, and XL structures, respectively. The normalizations are defined in Eqs. (30) and (31).

Scaling 3. Sheath resistivity regime

- Colisionless (sheath resistivity dominated) regime is realized when:

$$\min\left[1, \frac{\nu_{RT}^2\,\Omega_i}{\nu_{i,n}^3}, \frac{\nu_{RT}^2\,\Omega_i}{\left(\nu_{sink}-\nu_{src}\right)^3}\right] \gg \varphi \gg \max\left(\frac{\nu_{\blacklozenge}^{\frac{3}{2}}}{\nu_{RT}\,\Omega_i^{\frac{1}{2}}}, \frac{D_{e,i}+D_{e,n}}{\rho_s^2\,\Omega_i}, \frac{\eta_i}{\rho_s^2\,\Omega_i}\right).$$

- Then we have:

$$\chi_0 = 1, \quad \chi_{2_\blacklozenge} = \chi_{2_\perp} = \chi_4 = \sigma = 0, \quad \tau = \tau_i\left(\frac{\nu_{sink}^3\Omega_i}{\nu_{RT}^4}\right)^{\frac{1}{5}}, \qquad D = \frac{D_{e,i}+D_{e,n}}{\rho_s^2}\left(\frac{\nu_{sink}^3}{\nu_{RT}^4\,\Omega_i^4}\right)^{\frac{1}{5}}.$$

Sheath resistivity dominated (collisionless) regime

Ion density

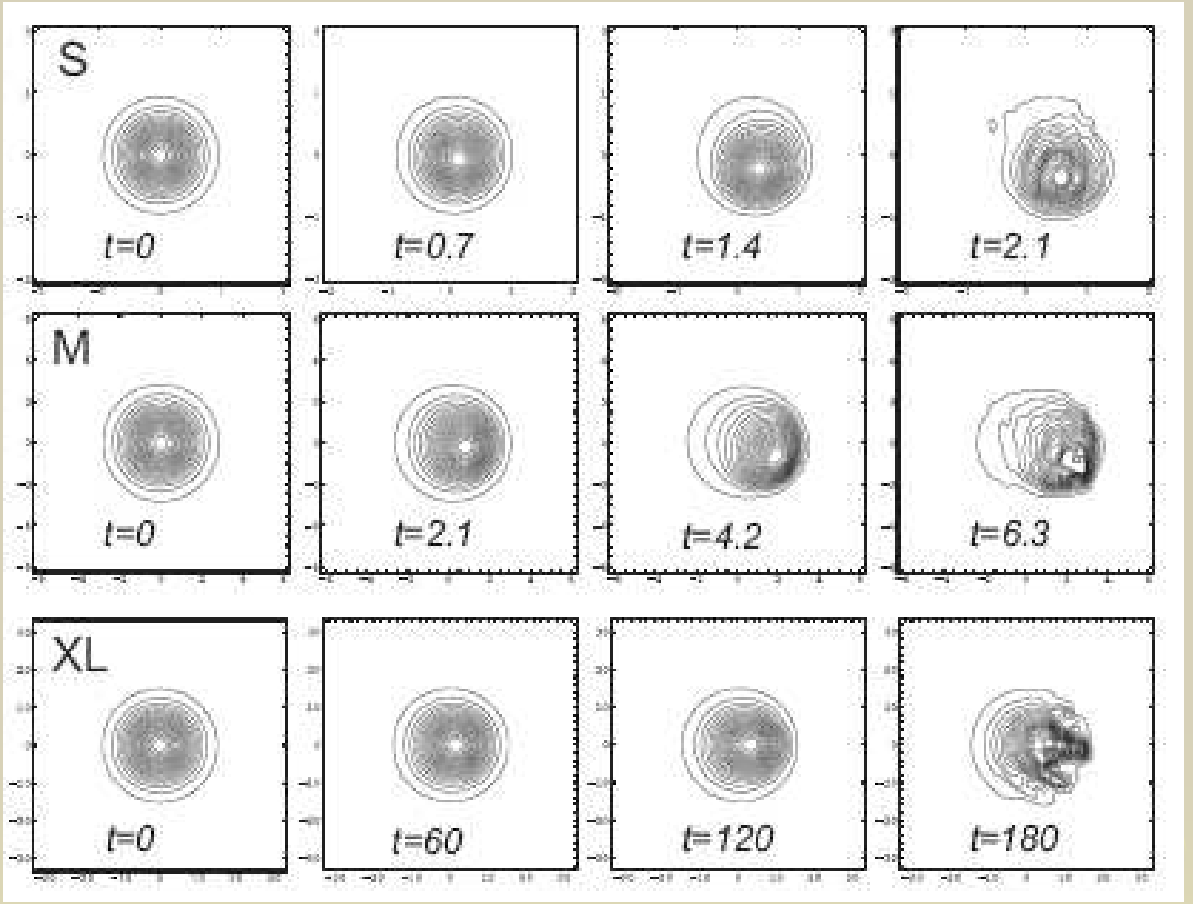

FIG. 3: The effect of the finite ion temperature on the blob dynamics in the **sheath connected** regime, in the vicinity of the wall of the vessel. From top to bottom are the S, M, and XL blob. We used $D = 10^{-3}$, $\chi_0 = 1$, $\chi_{2\perp} = \chi_{2\parallel} = \chi_4 = \gamma = \sigma = 0$, and the dimensionless ion temperature was adopted as $\tau = 1, 5$ and 5 for the S, M, and XL structures, respectively. The normalizations are defined in Eqs. (35) and (36).

Scaling laws 4. Viscous regime

- Viscosity (or ion-ion collision-) dominated regime is realized when:

$$\min\left[1, \left(\frac{\nu_{RT}^4}{\nu_{sink}^3\,\Omega_i}\right)^{\frac{1}{5}}, \frac{\nu_{RT}^2\,\Omega_i}{\nu_{i,n}^3}, \frac{\nu_{RT}^2\,\Omega_i}{\left(\nu_{sink}-\nu_{src}\right)^3}\right] \gg \varphi \gg \max\left(\frac{\nu_{\parallel}^{\frac{3}{2}}}{\nu_{RT}\,\Omega_i^{\frac{1}{2}}}, \frac{D_{e,i}+D_{e,n}}{\rho_s^2\,\Omega_i}\right).$$

- Then we have:

$$\chi_4 = 1, \quad \chi_0 = \chi_{2_\parallel} = \chi_{2_\perp} = \sigma = 0, \quad \tau = \tau_i\ \rho_s^2 \Omega_i / \eta_i,$$

$$D = (D_{e,i} + D_{e,n})/\eta_i.$$

Ion viscosity dominated regime

Ion density

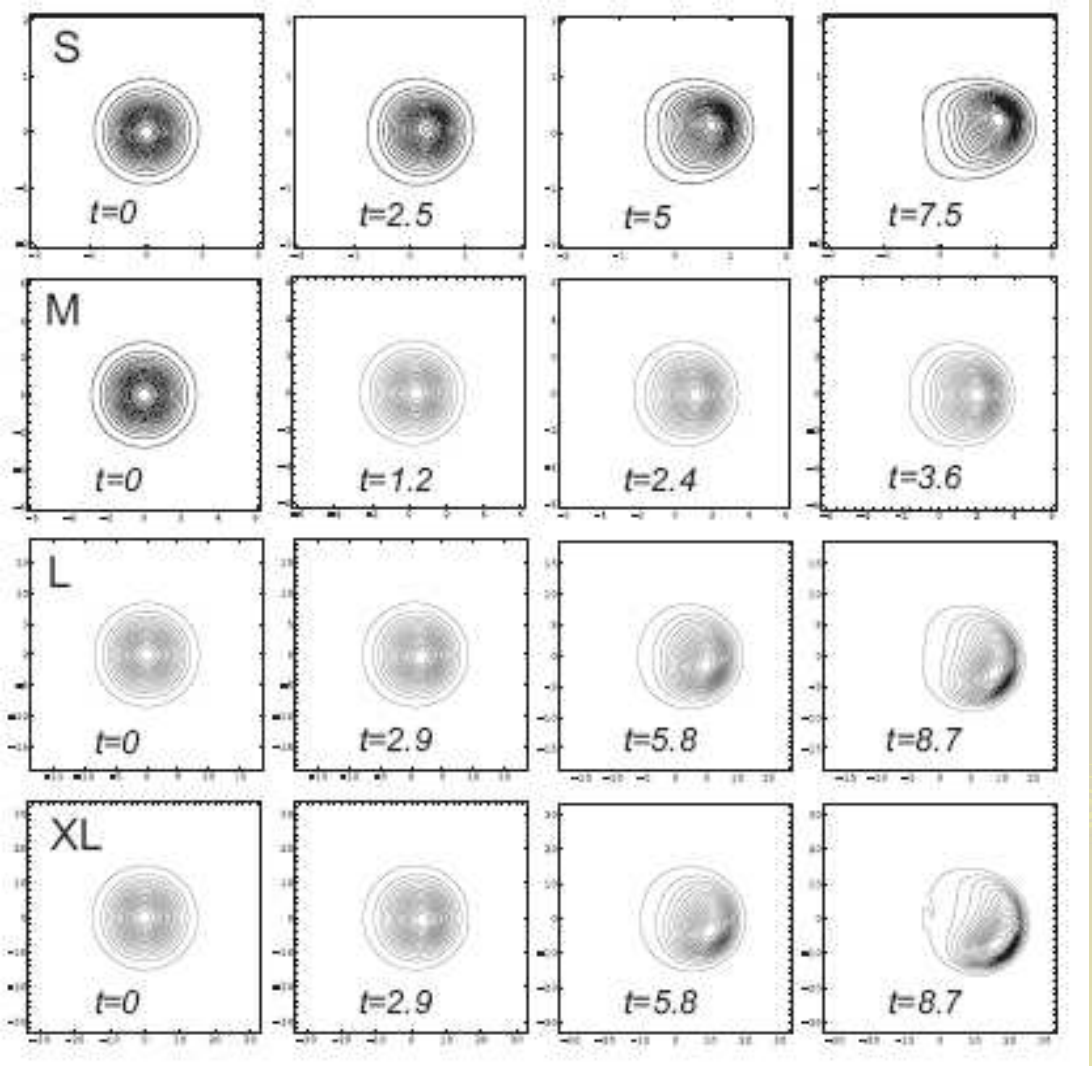

The effect of the finite ion temperature on the blob dynamics in the viscous regime. From top to bottom are the S, M, L, and XL blob.

Conclusions

- Our equations describe the nonlinear flute and drift perturbations in the presence of the magnetic curvature drive, convective nonlinearity, plasma sources and sinks, and dissipations arising from the electric current loss to the wall, electron-ion collisions, ion viscosity and collisions with neutrals. They include two new effects which fundamentally change the nonlinear behavior.
- All previous works considered cold ions. It is not a good approximation for tokamaks, in which the electron and ion temperatures in the plasma edge and SOL are close to each other.
- Finite ion temperature, besides some quantitative differences, introduced a qualitatively new effect in the ion vorticity equation. We neglected the ion temperature inhomogeneity, which may contribute to the turbulence via the linearly unstable ITG. The finite ion temperature cntribution may dominate the standard vorticity term considered previously.This new term also breaks the symmetry of the SOL blobs with cold ions, which feature monopole-like density and dipole-like potential profiles.
- We derived a new model for the parallel electron dynamics, using a rigorous separation of rapid and slow parallel variables, which gave a parallel diffusion term in the vorticity equation, in contrast to the 2-D diffusion associated with the ion-neutral collisions. Previously, the parallel dynamics was described by a linear model with effective wavenumber.

Conclusions (continued)

- Our approach also improves the description of the current loss to the wall, which is now related with the blob potential at the plasma-sheath boundary, and not by the local value. As a consequence, we obtain an intuitively expected result that the influence of the wall decreases with the distance. This corresponds to the increase of the blob radial velocity as they, at large distances, approach the inertial regime, which produces a bending and the eventual break up of the structure.
- Our numerical solutions reveal that the coupling with nonlinear drift modes introduces the collapse of the oblique blobs in the lateral direction, followed by a clockwise rotation and radial propagation. Both the finite ion temperature effects and the tilt of the structure in combination with the parallel resistivity produces the symmetry breaking of blobs, as compared with their 2-D, cold-ion counterparts. The symmetry breaking introduces a poloidal component in the blob velocity, while its overall stability properties and the speed are not affected qualitatively.
- In the future work, we will use our 3-D model with warm ions to study the ballooning/interchange turbulence at the core edge – the generation of shear flows and streamers (blobs). This requires only the change of boundary conditions.

Thank you for your attention!!